ARTICLE
Journal of Cellular Biochemistry 117:132–143 (2016)

Journal of Cellular Biochemistry

Chlamydia trachomatis Inclusion Disrupts Host Cell Cytokinesis to Enhance Its Growth in Multinuclear Cells

He Song Sun, Alex T.-W. Sin, Mathieu B. Poirier, and Rene E. Harrison*

Department of Biological Sciences, University of Toronto, 1265 Military Trail, Toronto, Ontario M1C 1A4, Canada

ABSTRACT

Chlamydia trachomatis, the leading cause of bacterial sexually transmitted infections, disrupts cytokinesis and causes significant multinucleation in host cells. Here, we demonstrate that multinuclear cells that result from unsuccessful cell division contain significantly higher Golgi content, an important source of lipids for chlamydiae. Using immunofluorescence and fluorescent live cell imaging, we show that *C. trachomatis* in multinuclear cells indeed intercept Golgi-derived lipid faster than in mononuclear cells. Moreover, multinuclear cells enhance *C. trachomatis* inclusion growth and infectious particle formation. Together, these results indicate that *C. trachomatis* robustly position inclusions to the cell equator to disrupt host cell division in order to acquire host Golgi-derived lipids more quickly in multinucleated progeny cells. J. Cell. Biochem. 117: 132–143, 2016.

KEY WORDS: CHLAMYDIA; MULTINUCLEATION; GOLGI; MITOSIS; CERAMIDE

The obligate intracellular pathogen, *Chlamydia trachomatis*, is the leading cause of bacterial sexually transmitted infections worldwide and epidemiological studies have suggested a link between *C. trachomatis* infection and higher risks of cervical cancer [WHO, 2001; Madeleine et al., 2007]. Chlamydiae exist in two distinct forms: the infectious elementary body (EB), which is well-suited for extracellular survival, and the non-infectious reticulate body (RB), which is the intracellular replicative form [Beatty et al., 1994]. Once chlamydiae enters a susceptible host cell, it resides in a host membrane-bound vacuole termed an inclusion, where EBs differentiate into RBs and begin to replicate [Hatch et al., 1984]. The size of the inclusion increases drastically over the course of the infection and the inclusion can occupy almost the entire host cytoplasm toward the end of the infection [Neeper et al., 1990; Hybiske and Stephens, 2007]. During later stages of the infection, RBs differentiate into EBs prior to exiting the host cell by lysis or extrusion [Hackstadt et al., 1997; Hybiske and Stephens, 2007]. The cysteine protease-mediated lytic pathway involves the rapid sequential permeabilization of inclusion, nuclear and plasma membranes, which ultimately kills the host cell [Hybiske and Stephens, 2007]. Unlike lysis, the chlamydial inclusion can also leave behind a viable host cell in a process termed extrusion [Beatty, 2007; Hybiske and Stephens, 2007]. Actin and myosin play essential roles in the extrusion pathway and the *C. trachomatis* inclusion can recruit an actin coat around itself [Hybiske and Stephens, 2007; Chin et al., 2012].

Chlamydiae exploit host amino acids, lipids and nucleotides to ensure its replication [Hatch, 1975; Tipples and McClarty, 1993; Hackstadt et al., 1995, 1996; Braun et al., 2008]. *C. trachomatis* disrupts the normal Golgi structure and recruits the fragmented Golgi stacks around the inclusion to gain increased access to host Golgi-derived lipids, which can significantly improve *C. trachomatis* replication rate in interphase cells [Heuer et al., 2009]. During mitosis, the Golgi undergoes a fragmentation process and becomes thousands of sub-micron vesicles that form the Golgi haze [Shima et al., 1998; Gaietta et al., 2006]. These Golgi vesicles are then partitioned into two daughter cells guided by the mitotic spindle [Shima et al., 1998; Wei and Seemann, 2009]. After the completion of cell division, two distinct Golgi stacks that are formed during cytokinesis fuse together to reform an intact Golgi in each daughter cell [Gaietta et al., 2006]. However, the fate and Golgi content within multinucleated cells has not been examined to date. This is particularly germane with respect to chlamydial infection, which can induce significant host cell multinucleation by blocking cleavage furrow ingression or abscission [Greene and Zhong, 2003; Sun et al., 2011; Brown et al., 2012]. *C. trachomatis* inclusions can localize to the cell equator, where cleavage furrows usually form and ingress, at a much higher frequency than similarly sized vacuole generated by internalized latex beads [Sun et al., 2011]. We have previously shown that Chlamydial protein synthesis contributes to the equatorial positioning of the inclusion during furrow ingression [Sun et al., 2011]. Moreover, *Chlamydia muridarum*, the murine

Grant sponsor: Canadian Institutes of Health Research; Grant number: MOP-68992.
*Correspondence to: Rene E. Harrison, Department of Biological Sciences, University of Toronto, 1265 Military Trail, Toronto, Ontario M1C 1A4, Canada. E-mail: harrison@utsc.utoronto.ca
Manuscript Received: 5 January 2015; Manuscript Accepted: 12 June 2015
Accepted manuscript online in Wiley Online Library (wileyonlinelibrary.com): 17 June 2015
DOI 10.1002/jcb.25258 • © 2015 Wiley Periodicals, Inc.

chlamydial species, can infect cells actively undergoing DNA synthesis and induce cell proliferation *in vivo* [Knowlton et al., 2013]. However, the advantage that Chlamydia can gain from disrupting host cell division remains unclear.

Here, we examine whether disrupting host mitosis confers any benefit to this bacterium. Using immunofluorescence (IF), live cell imaging and flow cytometry, we show that multinuclear cells that fail to divide contain higher Golgi content than mononuclear cells. Moreover, *C. trachomatis* can intercept Golgi-derived lipids more rapidly in multinuclear cells than in mononuclear cells. Multinuclear cells induced by siRNA knockdown of anillin and Ect2 allow enhanced *C. trachomatis* inclusion growth and infectious particle formation. Our work strongly suggests that *C. trachomatis* actively seeks to block host cell division to gain additional growth advantage in multinucleated cells.

MATERIALS AND METHODS

CELL CULTURE, *C. trachomatis* INFECTION, AND CELL SYNCHRONIZATION

HeLa and HEK cells cultured in DMEM supplemented with 10% fetal bovine serum were kept at 37°C with 5% CO_2. *C. trachomatis* L2 was a generous gift from Dr. Hackstadt (NIAID). To generate mitotic cells, HeLa cells were synchronized at 28 h postinfection (hpi) with 40 ng/ml nocodazole (Sigma–Aldrich) for 8 h to induce mitotic checkpoint. Cells synchronized into mitosis were subsequently released by two washes with DMEM and fixed after 55 min.

To generate large numbers of multinuclear cells for Golgi content quantification, HeLa cells were synchronized with 2 mM thymidine for 24 h into S-phase. Following thymidine washout, cells were synchronized with 40 ng/ml nocodazole for 14 h to obtain large numbers of mitotic cells. By the end of the nocodazole treatment, mitotic cells were tapped off from the culture flask, collected and washed twice. These mitotic cells were seeded onto 25 mm glass coverslips or T75 flasks pre-treated with poly-L-lysine to assist cell adhesion. Cells were released in drug-free media for 30 min before 100 μM blebbistatin was added to block furrow ingression. Blebbistatin was kept in the media for 3 h and then removed with five thorough washes. Cells were released for another 5 h to allow recovery from the blebbistatin treatment before fixation and subsequent IF or quantitative flow cytometry analysis.

LIVE CELL IMAGING

Asynchronous HeLa cells were seeded onto 35 mm glass-bottom dishes (MatTek) in DMEM and infected with *C. trachomatis* for 28–36 h before imaging. Live cell DIC imaging was conducted using Carl Zeiss AxioObserver Z1 epifluorescent microscope. The culturing environment was maintained at 37°C with 5% CO_2 using an incubator XL-S1 with TempModule S1, CO_2 module S1, and heating device humidity S1 (Carl Zeiss). Images were acquired using AxioCam MRm camera through 20x/0.8 Plan Apochromat air objective. The time-lapse DIC imaging was carried out once every 3 min for 24 h and fields of views with mitotic events were selected and a representative field was shown.

Cerulean-GalT was a gift from Dr. Jennifer Lippincott-Schwartz (Addgene plasmid #11930) and it was transfected into HeLa cells using FugeneHD 24 h before *C. trachomatis* infection [Cole et al., 1996]. *C. trachomatis*-infected HeLa cells were synchronized at 28 h postinfection for 8 h with 40 ng/ml nocodazole and released into fresh media. Images were acquired once every 2 min.

For live fluorescent ceramide trafficking experiments, infected HeLa cells were stained with DRAQ5 (Cell Signaling) for 10 min to label both the host and *C. trachomatis* DNA. Following the DNA stain, 35 mm culture dish containing *C. trachomatis*-infected HeLa cells was screened using a spinning disk confocal microscope with temperature and CO_2 control. Fields with both mononuclear and multinuclear cells were chosen and the imaging began as soon as BSA-complexed BODIPY FL C5-ceramide (Life Technologies) was added to the cells. The uptake of fluorescent ceramide into *C. trachomatis* inclusions was recorded once every 30 s for 30 min. The total fluorescence signal from the inside of the *C. trachomatis* inclusion was quantified by drawing along the inner edges of the inclusion using Volocity.

IMMUNOFLUORESCENCE AND QUANTIFICATION

Cells were fixed with ice cold methanol for 15 min for the immunostaining of Inc101 and γ-tubulin. Cells were fixed with 4% paraformaldehyde (PFA) for 20 min for the immunostaining of GM130, giantin, mannosidase II, HPA, GS-II, CERT, and α-tubulin. PFA-fixed cells were permeabilized for 20 min with 0.1% Triton X-100 in PBS with 100 mM glycine. Both methanol and PFA fixed cells were blocked with 5% fetal bovine serum in PBS for 1 h before they were incubated with γ-tubulin (1:200, Sigma–Aldrich), Inc101 (1:100, generous gift from Dr. Hackstadt), α-tubulin (1:500, Sigma–Aldrich), CERT (1:100, Sigma–Aldrich), GM130 (1:200, BD Biosciences), giantin (1:200, Abcam), and mannosidase II (1:200, Abcam), primary antibodies. Both primary and secondary antibody incubations were carried out for 1 h at room temperature. F-actin and DNA were visualized using phalloidin and DAPI, respectively. Lectins *Helix pomatia* agglutinin (HPA) and GS-II were incubated with cells according to manufacturer's protocol (Life Technologies).

For the quantification of inclusion localization, inclusion and host structures were labeled with DAPI and γ-tubulin staining. Inclusions were quantified as centrally located when they were positioned in between the segregating chromosome bands in telophase. Inclusions were quantified as centrally located when they reached across the equatorially located chromosome band during metaphase.

Golgi content in mononuclear and multinuclear HeLa cells was quantified using GM130 signal intensity. Epifluorescent images of mononuclear and multinuclear HeLa cells were acquired with identical exposure time and excitation intensity. GM130 fluorescence intensity in mononuclear and multinuclear cells was analyzed using ImageJ. The fold change in GM130 signal intensity was normalized against control cells, which went through the same synchronization procedure but did not receive the blebbistatin treatment.

The quantification of fluorescent ceramide acquisition in live infected HeLa cells was carried out using Volocity. The total fluorescent intensity in *C. trachomatis* inclusions by the end of the

live spinning disk confocal imaging was measured. Threshold for the quantification was defined such that only bacteria particles that have clearly defined shape were included, which excluded most of the background signal. The ceramide signal intensity in multinuclear cells was normalized against intensities in mononuclear cells to generate the fold changes. *C. trachomatis* inclusions in 31 pairs of mononuclear and multinuclear cells were compared.

To quantify *C. trachomatis* inclusion sizes in mononuclear and multinuclear cells, infected HeLa and HEK cells were randomly imaged and inclusion sizes in multinuclear and mononuclear cells were quantified using AxioVision. At least 170 HeLa and HEK cells were quantified in each category. To induce multinucleation, HeLa and HEK cells were transfected with anillin (Integrated DNA Technologies, HSC.RNAI.N018685.12.6) [Liu et al., 2012] or Ect2 siRNA (Life Technologies, 13778100) and infected with *C. trachomatis* at 24 h after siRNA transfection. Cells were fixed and immunostained using *C. trachomatis* antibody, phalloidin and DAPI at 48 h after transfection (data not shown). Inclusion sizes were measured using AxioVision.

To measure *C. trachomatis* IFU in mononuclear and multinuclear cells, HeLa cells were transfected with control, anillin or Ect2 siRNA and infected with identical numbers of *C. trachomatis* 24 h after transfection. Cells were lysed at 54 h after transfection (30 h after *C. trachomatis* infection) by harshly scraping the host cells in fresh culture media. Lysates were stored at −80°C and used to infect fresh HeLa cells. HeLa cells infected with control, anillin or Ect2-depleted lysates were fixed and immunostained for *C. trachomatis*, F-actin and DNA at 28 h postinfection. The number of inclusions was counted in more than 100 cells/experiment in three independent experiments.

Student's *t* test was used for all quantifications and $P < 0.05$ was used as the statistical significance cut-off.

RESULTS

C. trachomatis INCLUSIONS ARE FOUND AT THE CELL CENTER AS EARLY AS METAPHASE DURING CELL DIVISION

We have previously demonstrated in synchronized HeLa cells that *C. trachomatis* inclusions localize to the cell equator and block furrow ingression during telophase using fluorescent live cell imaging [Sun et al., 2011]. Synchronized cells had to be used for fluorescent live cell imaging due to significant phototoxicity and cell death associated with long-term imaging of asynchronous cultures. To confirm that central localization of inclusions during mitosis also occurred in asynchronous cells, we conducted long-term live DIC imaging experiments on *C. trachomatis*-infected HeLa cells. Multi-day DIC imaging of HeLa cells had no adverse effect on cell viability or division (data not shown). In asynchronous, naturally dividing cells, *C. trachomatis* inclusions still very frequently localized to the cell equator and prevented the completion of host cell division (Fig. 1A, left, arrows and Supplemental Movie S1). Based on our live DIC imaging, *C. trachomatis* inclusions appeared to localize to the cell equator, marked by the condensed chromosome band (Fig. 1A, right, arrows), as early as metaphase (Fig. 1A, right and Supplemental Movie S1). Since DIC imaging does not provide conclusive evidence of the relative positioning of the chromosome band and inclusion, we confirmed this observation with IF of synchronized cells in metaphase and telophase (Fig. 1B). Quantification of inclusion positioning in the two mitotic phases revealed that *C. trachomatis* inclusions localized to the cell equator in over 90% of the cells during both phases, suggesting that *C. trachomatis* inclusions already localized to the host cell equator as early as metaphase (Fig. 1C). Microdomains on *C. trachomatis* inclusion membrane have been shown to be in close proximity to the host centrosomes during both interphase and mitosis [Mital et al., 2010]. In our study, centrally located *C. trachomatis* inclusions were decorated by microdomains close to both centrosomes in host cells during metaphase (Fig. 1D). Together, these results indicate that the equatorial positioning of *C. trachomatis* inclusion in mitosis is consistently achieved before telophase and is possibly mediated by inclusion microdomains.

MULTINUCLEAR CELLS THAT FAIL TO DIVIDE RETAIN GOLGI APPARATUS MEANT FOR TWO DAUGHTER CELLS

Since Chlamydial protein synthesis played an important role in localizing the inclusion to the cell center to block host cell division [Sun et al., 2011], we next explored whether blocking host cell division conferred any physiological benefits to *C. trachomatis*. It has been well documented that the replicative success of *C. trachomatis* is highly dependent on access to host Golgi lipids [Heuer et al., 2009]. We first examined Golgi distribution in infected cells after successful or blocked mitosis using IF. In the rare instances when host cell mitosis was not blocked by the inclusion, approximately half of the total Golgi content was inherited by each daughter cell similar to un-infected cells (Fig. 2A). Consequently, the *C. trachomatis* inclusion would no longer have access to Golgi lipids in the other daughter cell upon successful completion of host cell division, unless the *C. trachomatis* inclusion also separates into two daughter cells. Based on our live cell imaging experiments, *C. trachomatis* inclusions rarely divided into two daughter cells, suggesting *C. trachomatis* would very often lose Golgi content to the uninfected daughter cell if the host were to successfully divide. In cells where *C. trachomatis* inclusions blocked the separation of the two daughter cells, the Golgi began to reform regardless of whether cleavage furrow ingression was completed (Fig. 2B). In addition, the blocked furrow eventually regressed and the Golgi content that was meant for two daughter cells was retained in a single infected cell. The presence of an internal midbody indicated that the cell recently failed to divide into two daughter cells. It was evident that the reformed Golgi in cells that failed to divide surrounded the *C. trachomatis* inclusion, similar to Golgi in mononuclear cells (Fig. 2B). Since it is difficult to ascertain the fate of Golgi stacks in fixed cells, we conducted long-term fluorescent imaging using nocodazole-synchronized HeLa cells transfected with Cerulean-GalT [Cole et al., 1996]. Through this method, we confirmed that *C. trachomatis*-infected HeLa cells that successfully divided into two daughter cells indeed distributed Golgi content into both daughter cells (Fig. 2C, top and Supplemental Movie S2). In cells that failed to divide due to the presence of *C. trachomatis* inclusions, the Golgi apparatus meant for two daughter cells was retained in a single multinuclear host cell and fused back into a single Golgi after the failed division (Fig. 2C, bottom and Supplemental Movie S3).

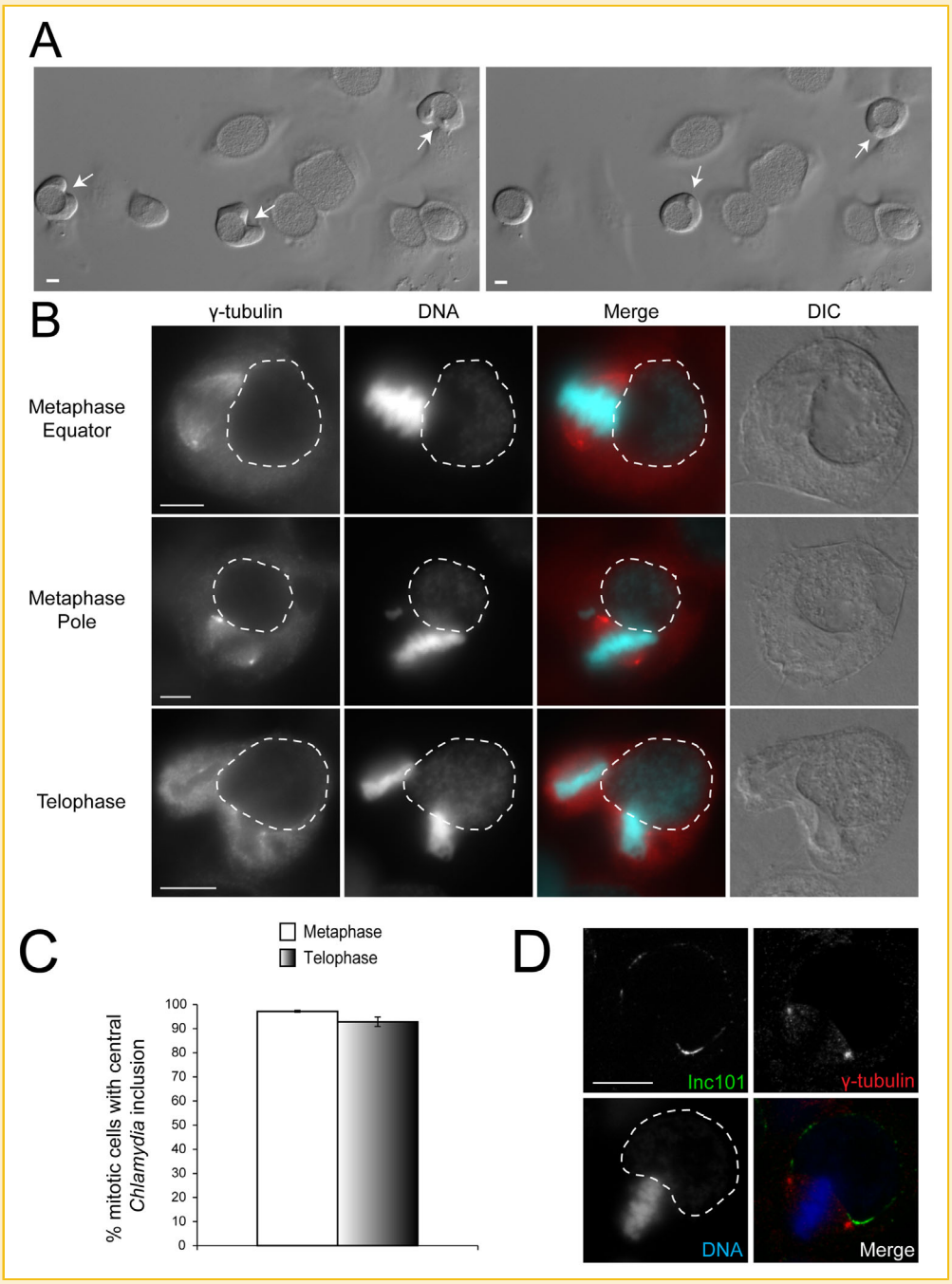

Fig. 1. *C. trachomatis* inclusions localize to the host cell centre by metaphase. A: Asynchronous HeLa cells infected by *C. trachomatis* were imaged using long-term live DIC imaging. Arrows indicate cells containing centrally located inclusions during telophase (left) and metaphase (right). B: *C. trachomatis*-infected HeLa cells were synchronized with low dose nocodazole for 8 h at 28 h postinfection and released for either 30 (metaphase) or 55 min (telophase) before fixation. Inclusion positioning was visualized with γ-tubulin (red) and DAPI (cyan) staining. Inclusions are outlined by white dotted lines. C: *C. trachomatis* inclusion positioning was quantified in both metaphase and telophase cells. Approximately 97% of metaphase and 93% of telophase cells contained centrally located inclusions at 36 hpi ($P > 0.2$). At least 50 cells were quantified for each mitotic phase per experiment. Error bars represent SEM from three independent experiments. D: Microdomains, revealed by Inc101 staining, on centrally located *C. trachomatis* inclusion were in close association with the host centrosomes during metaphase. Scale bars = 10 μm.

To ensure this was not a cell line-specific defect, we confirmed Golgi distribution in several human (MCF10A and HEK293) and mouse (NIH3T3) cell lines (Fig. 2D). In all the cell lines examined, the Golgi in infected multinuclear cells always surrounded the inclusion as observed in mononuclear cells (Fig. 2D). Furthermore, we confirmed that Golgi surrounded *C. trachomatis* inclusions in multinuclear cells with additional *cis* (giantin), *cis-medial* (HPA) and *medial-trans* (Mannosidase II and GS-II) markers [Suzaki and Kataoka, 1992; Velasco et al., 1993; Wasano et al., 1988; Follit et al., 2006, 2008; Jiang et al., 2006] (Fig. 3).

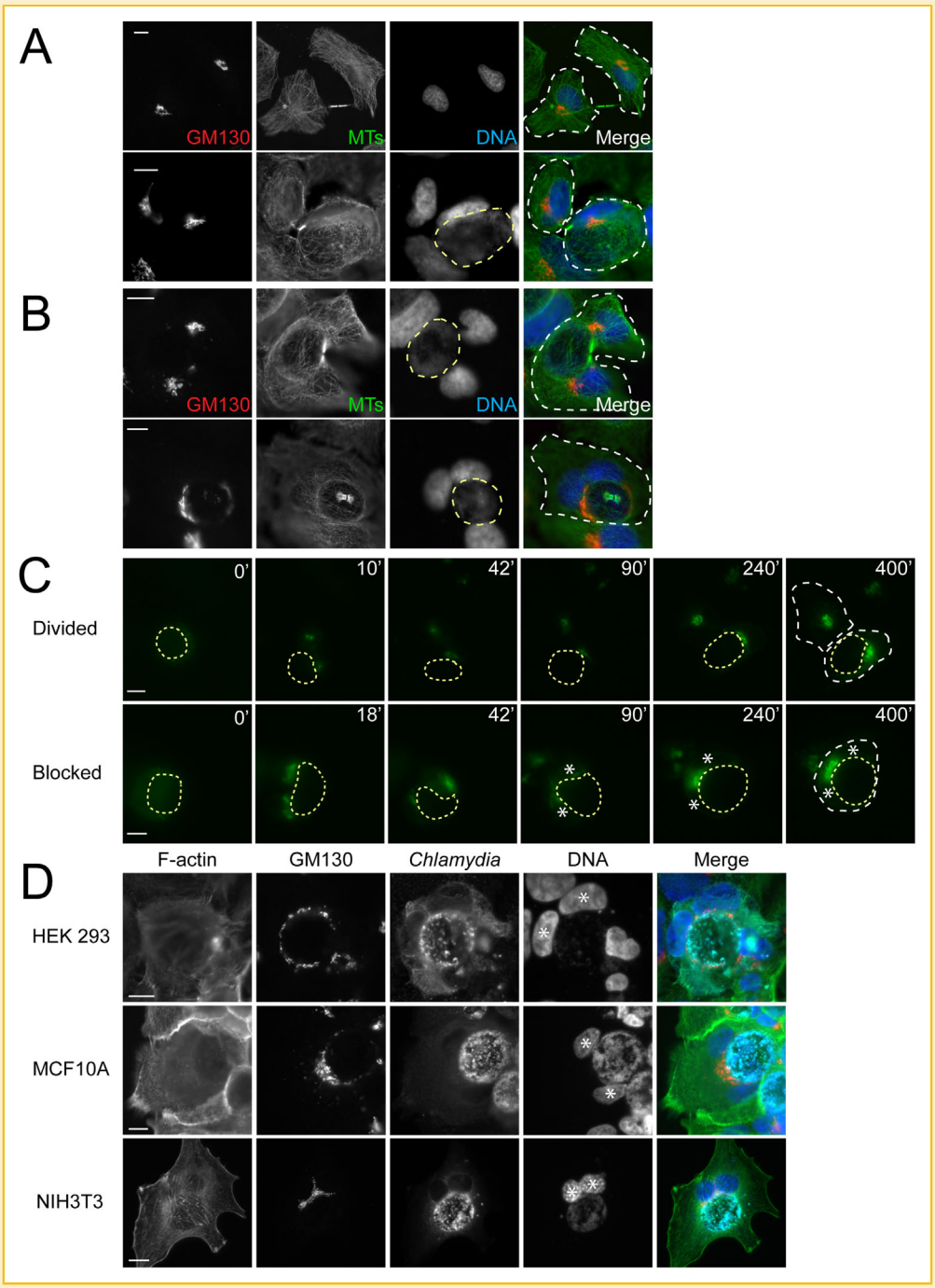

Fig. 2. *C. trachomatis* inclusions co-opt the entire Golgi apparatus when host mitosis is blocked. A: After a recent division event, marked by intense midbody α-tubulin (green) staining, each daughter cell inherited part of the Golgi indicated by GM130 staining (red). In the rare instances where *C. trachomatis* inclusion did not block furrow ingression, the uninfected daughter cell inherited part of the Golgi apparatus. *C. trachomatis* inclusion is marked by the yellow dotted line as revealed by DAPI staining (blue) and the host cell boundaries are marked by white dotted lines. B: In most *C. trachomatis*–infected telophase cells, the Golgi stacks began to reform even though furrow ingression was blocked by the inclusion. The prominent internal midbody indicated a multinuclear cell that recently failed to divide into two daughter cells. This multinuclear cell also contained fragmented Golgi stacks that surrounded the *C. trachomatis* inclusion. C: HeLa cells transfected with Cerulean-GalT were infected with *C. trachomatis* for 28 h and synchronized with 40 ng/ml nocodazole for 8 h and released into fresh media immediately before fluorescent live-cell imaging. Infected cells that successfully divided into two daughter cells distributed Golgi into both daughter cells (top), while Golgi was retained in a single multinuclear cell if the host cell mitosis was blocked (bottom). The *C. trachomatis* inclusions are identified by DIC (Supplementary Movies S2 and S3) and marked by yellow dotted lines and host cell boundaries are indicated by white dotted lines. Numbers indicate minutes and asterisks mark the nuclei in multinuclear cells. D: The Golgi apparatus (red) in multinuclear HEK293 (human fibroblast), MCF10A (human epithelial) and NIH3T3 (mouse fibroblast) cells (green, F-actin; blue, DNA) surrounded the *C. trachomatis* inclusions (cyan). Asterisks mark the nuclei in multinuclear cells. Scale bars = 10 μm.

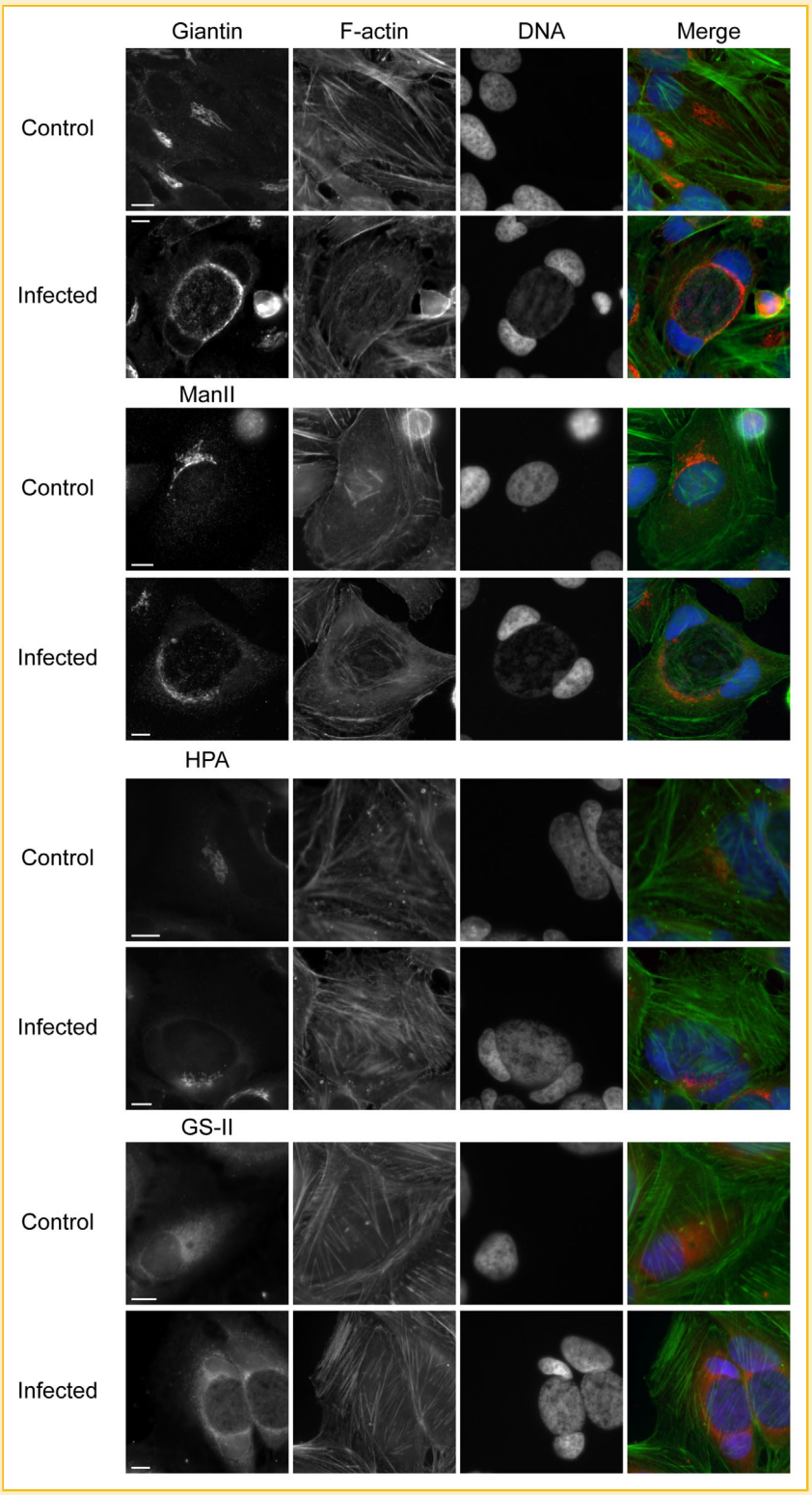

Fig. 3. *Cis*, *medial*, and *trans* Golgi stacks all surround the *C. trachomatis* inclusion in multinuclear cells. HeLa cells (F-actin, green; DNA, blue) infected with *C. trachomatis* were fixed at 36 hpi with PFA and immunostained with anti-giantin or mannosidase II (ManII) antibodies (red). HPA or GS-II lectins (red) were used to stain *cis-medial* and *medial-trans* Golgi stacks, respectively. Scale bars = 10 μm.

MULTINUCLEAR CELLS THAT FAIL TO DIVIDE CONTAIN INCREASED GOLGI CONTENT

In order to quantitatively measure the degree to which Golgi content was increased in cells that failed to divide, we artificially created cells that failed to divide. In this analysis, we did not use *C. trachomatis* to generate multinuclear cells, because *C. trachomatis* was known to modify Golgi structure and intercept Golgi content, which could interfere with the Golgi content measurement [Heuer et al., 2009]. Instead, we used a previously described synchronization procedure [Whitfield et al., 2002] and the resulting mitotic cells were either untreated or treated with blebbistatin to block furrow ingression. After a period of recovery, cells were fixed and stained for GM130 to label the Golgi. Both mononuclear and multinuclear cells were generated under both untreated and blebbistatin-treated conditions (Fig. 4A). Inspection of epifluorescent images revealed that multinuclear cells appeared to have physically larger Golgi apparatus than mononuclear cells (Fig. 4A). Quantification of GM130 signal intensity using IF images revealed that multinuclear cells contained approximately twice the amount of Golgi compared to mononuclear cells (Fig. 4B). In order to more accurately measure the total GM130 protein level/cell, we synchronized HeLa cells with thymidine for 24 h and then released the cells into low-dose nocodazole overnight to generate large numbers of mitotic cells for flow cytometry analysis. Mitotic cells were released from nocodazole

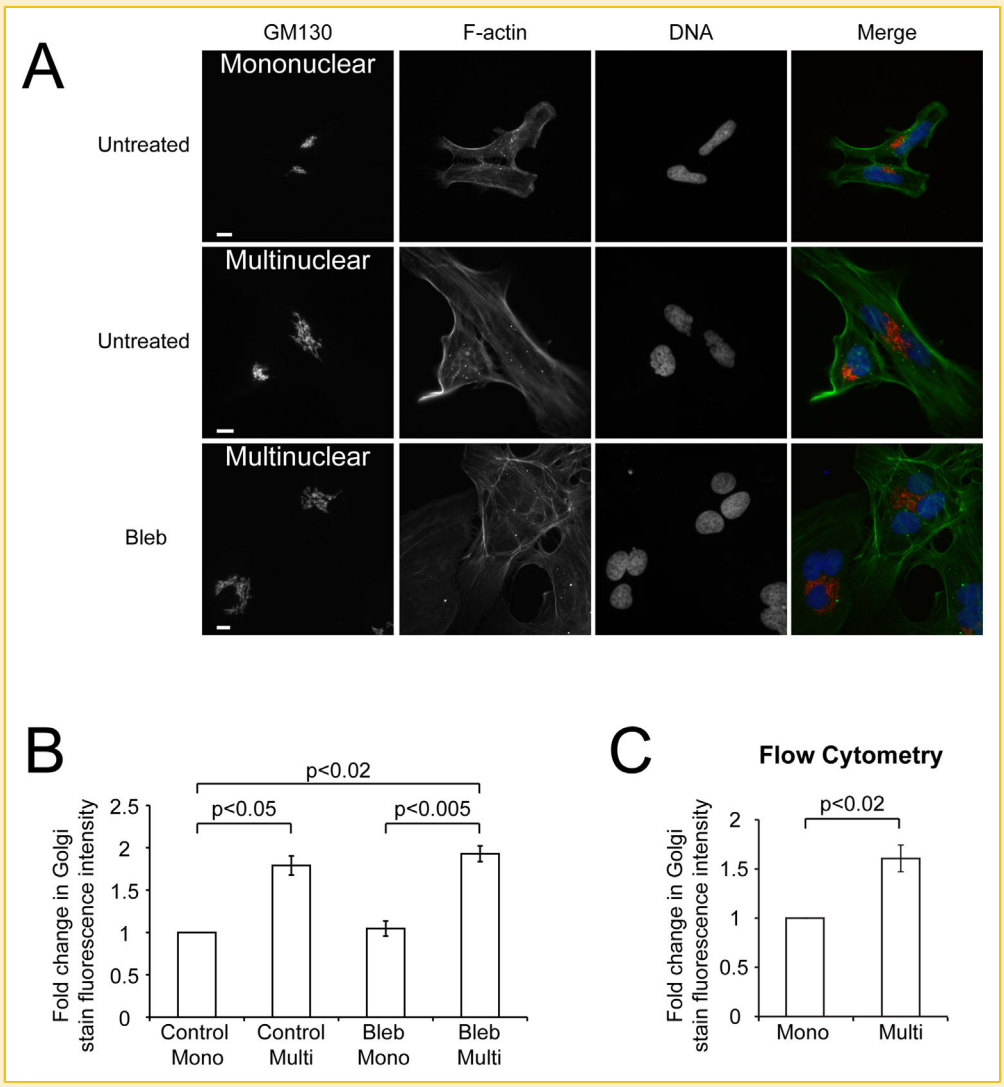

Fig. 4. Golgi content increases in multinuclear cells that fail to divide. A: Cells were synchronized into mitosis and then treated with blebbistatin to inhibit furrow ingression to generate large numbers of multinuclear cells. The resulting cells were fixed and stained for F-actin (green), Golgi (GM130, red), and DNA (blue). Scale bars = 10 μm. B: Quantification of GM130 signal intensity in IF images of mononuclear and multinuclear cells revealed that multinuclear cells contained significantly more Golgi protein than mononuclear cells. C: Cells were synchronized into mitosis with thymidine and low dose nocodazole and released in the absence (control group) or presence (treated group) of blebbistatin to generate cells that have recently undergone mitosis. Cells were fixed by methanol, stained by propidium iodide and GM130 antibody to label DNA and Golgi content, respectively. Cells were gated based on their DNA content with 2N cells in the control group being the mononuclear cells and 4N cells in the blebbistatin-treated group being multinuclear cells. Based on three independent flow cytometry experiments, the GM130 content increased by approximately 60% in multinuclear cells compared to mononuclear cells. Error bars represent SEM of three independent experiments.

for 30 min and then treated with blebbistatin to induce multinucleation. Following this procedure, approximately 90% of cells became multinuclear based on immunofluorescent images (data not shown). Cells were then fixed with methanol and stained with propidium iodide and GM130 antibody. There was a significant increase in GM130 content in multinuclear cells compared with mononuclear cells that went through the same synchronization procedure except blebbistatin (Fig. 4C). Together, these results suggest that on average multinuclear cells that fail to divide into two daughter cells indeed contain significantly more Golgi content than mononuclear cells.

C. trachomatis INTERCEPTS GOLGI-DERIVED LIPIDS MORE RAPIDLY IN MULTINUCLEAR CELLS COMPARED TO MONONUCLEAR CELLS

In order to determine whether *C. trachomatis* can acquire Golgi-derived nutrients more rapidly in cells that failed division, we conducted spinning disk confocal live cell imaging to monitor fluorescent BODIPY-ceramide trafficking to the inclusion [Heuer et al., 2009]. Ceramide is trafficked from Golgi to *C. trachomatis* particles inside the inclusion and disruption of host Rab proteins can result in dramatic decrease in ceramide targeting to the inclusion [Heuer et al., 2009; Rejman Lipinski et al., 2009; Capmany and Damiani, 2010]. HeLa cells seeded on glass-bottom dishes were infected with *C. trachomatis* for 36 h and fields containing both multinuclear and mononuclear cells were chosen. Imaging was started as soon as the fluorescent ceramide was added to the cells and the trafficking to *C. trachomatis* particles inside the inclusions were monitored in mononuclear and multinuclear cells. In order to label individual *C. trachomatis* particles, we pre-incubated infected cells with DRAQ5 for 10 min [Sun et al., 2012]. Through these live imaging experiments, we consistently observed that individual bacterial particles in multinuclear cells obtained fluorescent ceramide signals more rapidly than those in mononuclear cells within the same imaging field (Supplemental Movie S4 and Fig. 5A). The number of brightly labeled *C. trachomatis* particles appeared to be much higher in multinuclear cells compared to mononuclear cells, even though the inclusion sizes were comparable. Quantification of the total ceramide fluorescence intensity in *C. trachomatis* inclusions revealed that inclusions acquired ceramide much more rapidly in multinuclear cells than in mononuclear cells (Fig. 5B). Next, we wanted to examine whether the levels of non-vesicular ceramide transport protein, CERT, were also increased in chlamydia-induced multinuclear cells compared to infected mononuclear cells, as this protein is recruited to *C. trachomatis* inclusion membranes and is important for chlamydia growth [Derre et al., 2011; Elwell et al., 2011]. HeLa cells infected by *C. trachomatis* were stained with an anti-CERT antibody and analyzed using immunofluorescence microscopy with identical excitation light intensity and exposure time (Fig. 5C). CERT was strongly recruited to the *C. trachomatis* inclusion surface as previously reported (Fig. 5C) [Derre et al., 2011]. Quantification of CERT protein levels based on fluorescence intensity in extended focus images revealed that *C. trachomatis*-infected multinuclear cells contained significantly higher CERT content than infected mononuclear cells (Fig. 5D). These results indicate that the generation of multinuclear cells through blocking host cell division could indeed enhance lipid nutrient acquisition by *C. trachomatis*, which could in turn confer growth advantage to the bacteria.

C. trachomatis REPLICATES FASTER IN MULTINUCLEAR CELLS

To determine whether multinuclear cells that failed cell division could enhance *C. trachomatis* growth, we first examined *C. trachomatis* inclusion sizes in mononuclear and multinuclear HeLa and HEK cells (Fig. 6A). Quantification of inclusion areas revealed that *C. trachomatis* inclusions in multinuclear cells were significantly larger than in mononuclear cells for both cell lines (Fig. 6A). To confirm that having multinuclear host cells can indeed benefit *C. trachomatis* growth, we induced host cell multinucleation using siRNA against anillin, an important protein involved in cleavage furrow formation and stabilization [Piekny and Glotzer, 2008; Liu et al., 2012]. HeLa cells were transfected with anillin siRNA to induce multinucleation 24 h before *C. trachomatis* infection. Infected cells were fixed at 24 h postinfection (48 h post-siRNA transfection) and stained to measure inclusion sizes. IF analysis and quantification showed that approximately 85% of cells were multinucleated (data not shown) and *C. trachomatis* inclusions in multinuclear cells were significantly larger than those in mononuclear cells, which underwent identical transfection treatment (Fig. 6B, left). In addition, we measured the number of *C. trachomatis* inclusion forming units (IFUs) in mononuclear cells and multinuclear cells using a re-infection assay. HeLa cells were transfected with either scrambled (control) siRNA or siRNA against anillin 24 h before *C. trachomatis* infection and were lysed at 30 h postinfection (54 h post-siRNA transfection). Lysates were stored at −80°C and subsequently used to infect fresh HeLa cells to quantify how many infectious EBs (IFUs) were produced in control and multinuclear cells. Fresh HeLa cells infected with either control or anillin-depleted lysate were fixed at 28 h post-infection and stained to quantify the number of inclusions that formed. This re-infection assay showed that *C. trachomatis* replicated significantly faster in anillin-depleted multinuclear cells than in control cells (Fig. 6B, right). To ensure that *C. trachomatis* growth enhancement was not an anillin-specific artifact, we also generated multinuclear cells using an unrelated siRNA against Ect2, an important guanine nucleotide exchange factor for cleavage furrow ingression [Su et al., 2011]. Similarly, we observed that *C. trachomatis* produced significantly larger inclusions and higher IFUs in Ect2-depleted multinuclear cells than in mononuclear cells (Fig. 6C). To ensure that *C. trachomatis* growth enhancement was not a HeLa-specific artifact, we repeated the siRNA experiments in HEK cells to generate multinuclear cells. *C. trachomatis* inclusions in siRNA-induced multinuclear HEK cells were also significantly larger than those in mononuclear cells (Fig. 6D).

DISCUSSION

We have previously demonstrated that *C. trachomatis* inclusions localize very efficiently to the host cell center during telophase using live imaging and IF in synchronized cells [Sun et al., 2011]. In the current study, we confirmed these observations with live cell DIC imaging in asynchronous cells. Consistent with our previous report,

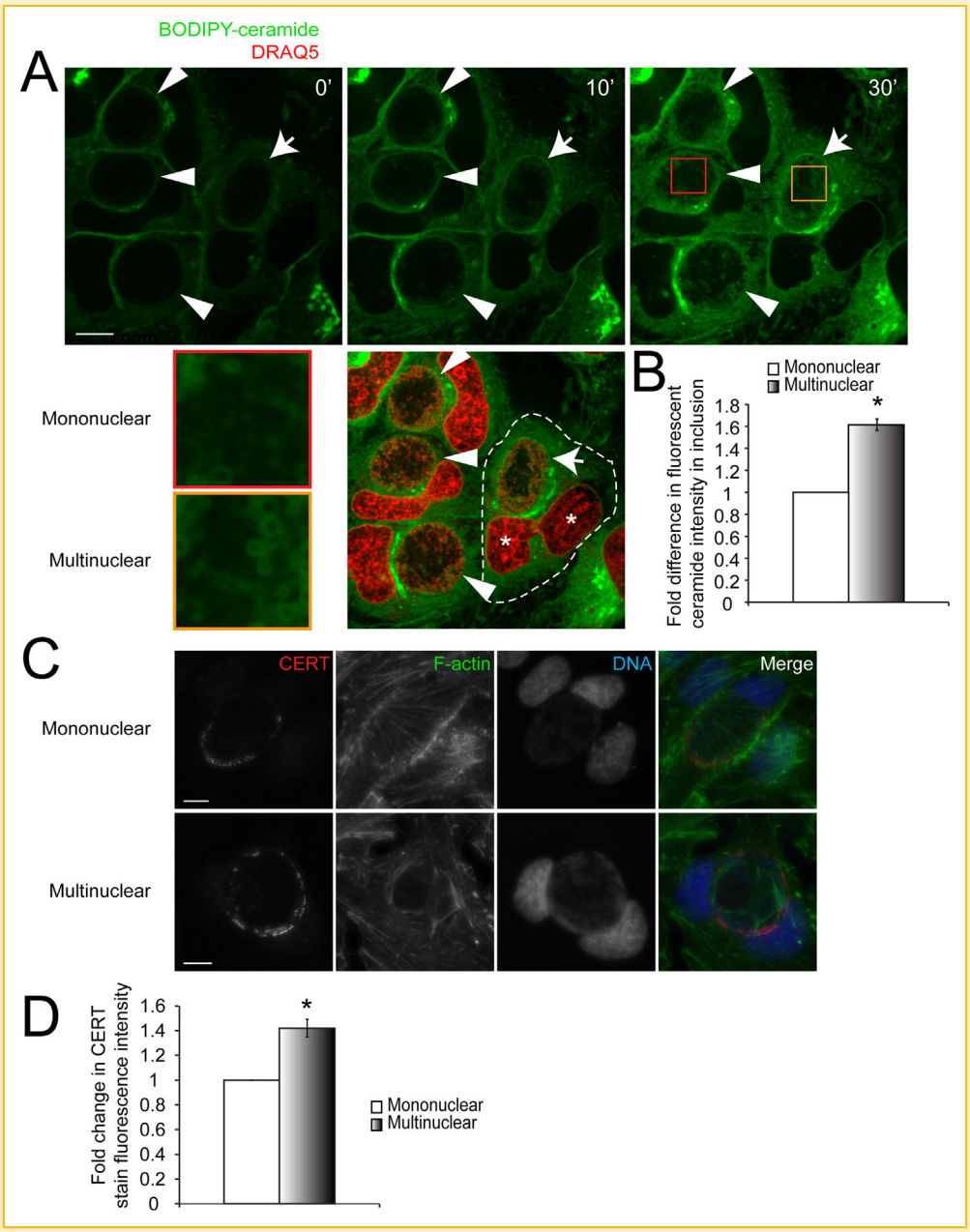

Fig. 5. C. *trachomatis* inclusions can acquire fluorescent Golgi-derived lipid markers more rapidly in multinuclear cells than in mononuclear cells. A: *C. trachomatis*-infected cells were imaged immediately after the addition of fluorescent ceramide (green) to determine the rate of lipid acquisition by inclusions. *C. trachomatis* inclusions and host nuclei were revealed by DNA stain (DRAQ5, red). Outline of the multinuclear cell is indicated by dotted line. Arrowheads mark the inclusions in single nuclear cells, while arrow indicates inclusion in multinuclear cell. Numbers indicate minutes after addition of ceramide and white asterisks indicate nuclei in the multinuclear cell. B: Quantification of fluorescence intensity inside *C. trachomatis* inclusions showed that *C. trachomatis* particles can intercept Golgi-derived lipids significantly faster in multinuclear cells than in mononuclear cells. A total of 31 pairs of infected mononuclear and multinuclear cells were quantified. Error bars represent SEM from three independent experiments. Black asterisk indicates $P < 0.05$. C: *C. trachomatis*-infected HeLa cells were stained for CERT (red), F-actin (green), and DNA (blue). Z-stack images were acquired using identical step-size, exposure time, and excitation light intensity. Representative extended-focus images are shown. Scale bars = 10 μm. D: CERT fluorescence intensities in infected cells were quantified using extended-focus images. There was a significant (42%) increase in CERT protein levels in *C. trachomatis*-infected multinuclear cells compared to mononuclear cells. Black asterisk indicates $P < 0.05$.

C. trachomatis inclusions in asynchronous cells also localized to the cell center very frequently, blocked furrow ingression and induced the formation of multinuclear host cells. The long-term DIC imaging did not involve the use of any synchronization agents and it did not cause detectable levels of phototoxicity-associated cell death; therefore, these results are the most accurate description of mitotic defects caused by *C. trachomatis*. In the current study, we observed that 97% of metaphase cells contain centrally located *C. trachomatis* inclusions indicating that *C. trachomatis* inclusions did not have to re-locate to the host cell center during anaphase or telophase.

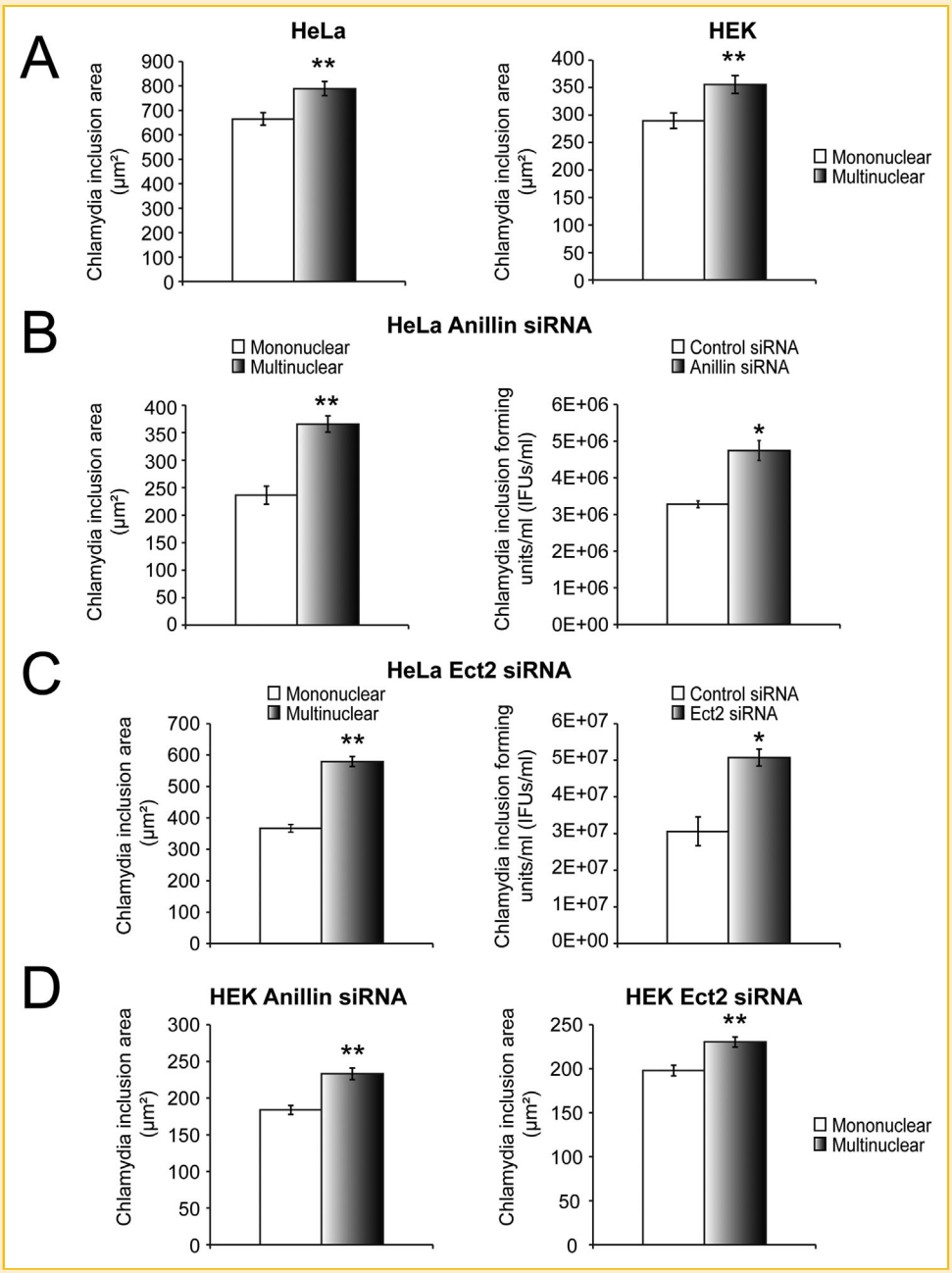

Fig. 6. C. *trachomatis* replicates faster in multinuclear cells that fail to divide. A: *C. trachomatis* inclusion sizes in mononuclear and multinuclear cells were compared in HeLa and HEK cells at 48 h after infection. Error bars represent SEM of *C. trachomatis* inclusion sizes in at least 170 mononuclear and multinuclear cells. B: HeLa cells were transfected with scrambled (control) or anillin siRNA and infected with *C. trachomatis* 24 h later. Cells were fixed and immunostained at 48 h after transfection (24 h after *C. trachomatis* infection). The *C. trachomatis* inclusion sizes were measured using immunofluorescence images. For *C. trachomatis* inclusion forming unit (IFU) quantification, control or anillin siRNA transfected cells were lysed by harsh scraping at 54 h after transfection (30 h after infection) and lysates were used to infect fresh HeLa cells to quantify IFUs. Fresh HeLa cells were infected for 28 h before fixation. At least 100 cells were quantified per experiments and three independent experiments were conducted. C: The same experiments described in (B) were repeated with Ect2 siRNA. (D) HEK cells were transfected with anillin or Ect2 siRNA and inclusion sizes in mononuclear cells and multinuclear cells were compared. At least 170 cells in each category were quantified. Error bars represent SEM. Single asterisks indicate $P < 0.05$ and double asterisks indicate $P < 0.01$.

It has been well documented that *C. trachomatis* infection can lead to host cell multinucleation by disrupting host cytokinesis through disruption of furrow ingression or abscission [Greene and Zhong, 2003; Sun et al., 2011; Brown et al., 2012]. Moreover, a recent study has shown that *C. muridarum* can infect actively replicating host cells in a mouse model [Knowlton et al., 2013]. Our study is the first to demonstrate that there is a physiological benefit for *C. trachomatis* to block host mitosis. Golgi content, measured by GM130 staining, was increased by approximately 90% in cells that failed to divide compared to mononuclear cells that went through the same synchronization protocol and successfully divided. Moreover, our quantitative flow cytometry analysis also confirmed that

multinuclear cells contained approximately 60% more GM130 protein than mononuclear cells. To our knowledge, this is the first study comparing Golgi content in multinuclear and mononuclear cells. Even though we have demonstrated that the per cell Golgi content increased in multinuclear cells compared to mononuclear cells, this was likely part of an overall protein content increase in multinuclear cells, which could also contain significantly higher levels of other organelles. Golgi and other organelles are partitioned into two daughter cells during mitosis under normal conditions [Altan-Bonnet et al., 2006; Gaietta et al., 2006; Wei and Seemann, 2009]. Following mitosis, the Golgi is reformed by the fusion of two distinct Golgi stacks into a common stack in each daughter cell [Gaietta et al., 2006]. Similar to uninfected cells, *C. trachomatis*-infected cells that successfully divided into two daughter cells distributed Golgi into each daughter cell. Consequently, based on our live and fixed imaging studies, *C. trachomatis* lost access to approximately half of the Golgi after completion of cytokinesis. In a cell whose cytokinesis was blocked, we observed that Golgi was retained in a single multinuclear cell and the reformed *cis*, *medial*, and *trans*-Golgi stacks all surrounded the *C. trachomatis* inclusion as it would in a mononuclear cell [Heuer et al., 2009]. The theory that *C. trachomatis* can retain more Golgi content by preventing host cell division is also in line with previous observations that *C. trachomatis* infection leads to delayed mitotic entry and prolonged cell cycle [Balsara et al., 2006; Knowlton et al., 2011]. By causing the host to enter mitosis less frequently, *C. trachomatis* also reduces the chance to lose half of the host Golgi content to one of the uninfected daughter cells.

Fluorescent ceramide has been commonly used to measure the rate of Golgi-derived lipid uptake by *C. trachomatis* in infected cells and several host factors important for *C. trachomatis* lipid acquisition, such as Rab 6, Rab 11, and CERT, have been identified using this method [Rejman Lipinski et al., 2009; Derre et al., 2011; Elwell et al., 2011]. Disruption of Golgi structures and normal trafficking can lead to significantly increased fluorescent ceramide accumulation in the inclusions [Heuer et al., 2009; Rejman Lipinski et al., 2009; Elwell et al., 2011]. Our current study took advantage of this well-established method and showed that inclusions in multinuclear cells acquired fluorescent ceramide much more rapidly than those in mononuclear cells. This indicates that inclusions can acquire lipids, an essential nutrient that can directly affect *C. trachomatis* replication [Heuer et al., 2009], faster in multinuclear cells that have failed to divide. In addition to sphingolipids visualized by fluorescent ceramides, *C. trachomatis* can intercept cholesterol from both the host plasma membrane and the Golgi [Pagano et al., 1991; Carabeo et al., 2003]. Extraction of cholesterol from the host plasma membrane using methyl-β-cyclodextrin caused a significant reduction in cholesterol trafficking to the *C. trachomatis* inclusion [Carabeo et al., 2003]. Interestingly, during the initial invasion stage of the infection, host cholesterol depletion by methyl-β-cyclodextrin significantly impacted *C. trachomatis* entry [Jutras et al., 2003; Gabel et al., 2004]. In addition, we artificially induced multinucleation in host cells using siRNA against anillin or Ect2, important proteins for cleavage furrow formation and ingression [Piekny and Glotzer, 2008; Su et al., 2011; Liu et al., 2012]. Our results indicated that *C. trachomatis* inclusions were significantly larger in multinuclear cells than in mononuclear cells. Moreover, *C. trachomatis* IFUs in anillin or Ect2-depleted multinuclear cells were significantly higher than that in control cells. Together, these results demonstrate that *C. trachomatis* indeed have a growth advantage in multinuclear host cells compared with mononuclear host cells.

In summary, *C. trachomatis* infection induces the formation of multinuclear host cell and efficiency of *C. trachomatis* to cause this defect is enhanced by the presence of bacterial protein synthesis [Greene and Zhong, 2003; Sun et al., 2011; Brown et al., 2012]. Our results demonstrate that *C. trachomatis* inclusions have a lipid acquisition and growth advantage when they reside in host cells that failed to divide. These findings strongly suggest that *C. trachomatis* actively seeks the host cell center during host mitosis to gain additional growth advantage. With the exciting emergence of novel genetic manipulation techniques for *C. trachomatis* [Kari et al., 2011; Wang et al., 2011], it will be interesting to systematically assess single-protein knock-out mutants to determine which *C. trachomatis* proteins are important for inclusion positioning and blocking host cell mitosis.

ACKNOWLEDGMENTS

This project is funded by a MOP-68992 grant from Canadian Institutes of Health Research (CIHR) to R.E.H. R.E.H. is a recipient of a CIHR New Investigator Award and an Ontario Early Researcher Award. The authors declare no conflict of interest.

REFERENCES

Altan-Bonnet N, Sougrat R, Liu W, Snapp EL, Ward T, Lippincott-Schwartz J. 2006. Golgi inheritance in mammalian cells is mediated through endoplasmic reticulum export activities. Mol Biol Cell 17:990–1005.

Balsara ZR, Misaghi S, Lafave JN, Starnbach MN. 2006. *Chlamydia trachomatis* infection induces cleavage of the mitotic cyclin B1. Infect Immun 74:5602–5608.

Beatty WL, Morrison RP, Byrne GI. 1994. Persistent chlamydiae: From cell culture to a paradigm for chlamydial pathogenesis. Microbiol Rev 58:686–699.

Beatty WL. 2007. Lysosome repair enables host cell survival and bacterial persistence following *Chlamydia trachomatis* infection. Cell Microbiol 9:2141–2152.

Braun PR, Al-Younes H, Gussmann J, Klein J, Schneider E, Meyer TF. 2008. Competitive inhibition of amino acid uptake suppresses chlamydial growth: Involvement of the chlamydial amino acid transporter BrnQ. J Bacteriol 190:1822–1830.

Brown HM, Knowlton AE, Grieshaber SS. 2012. Chlamydial infection induces host cytokinesis failure at abscission. Cell Microbiol 14:1554–1567.

Capmany A, Damiani MT. 2010. *Chlamydia trachomatis* intercepts Golgi-derived sphingolipids through a Rab14-mediated transport required for bacterial development and replication. PLoS ONE 5:e14084.

Carabeo RA, Mead DJ, Hackstadt T. 2003. Golgi-dependent transport of cholesterol to the *Chlamydia trachomatis* inclusion. Proc Natl Acad Sci USA 100:6771–6776.

Chin E, Kirker K, Zuck M, James G, Hybiske K. 2012. Actin recruitment to the Chlamydia inclusion is spatiotemporally regulated by a mechanism that requires host and bacterial factors. PLoS ONE 7:e46949.

Cole NB, Smith CL, Sciaky N, Terasaki M, Edidin M, Lippincott-Schwartz J. 1996. Diffusional mobility of Golgi proteins in membranes of living cells. Science 273:797–801.

Derre I, Swiss R, Agaisse H. 2011. The lipid transfer protein CERT interacts with the Chlamydia inclusion protein IncD and participates to ER-Chlamydia inclusion membrane contact sites. PLoS Pathog 7:e1002092.

Elwell CA, Jiang S, Kim JH, Lee A, Wittmann T, Hanada K, Melancon P, Engel JN. 2011. *Chlamydia trachomatis* co-opts GBF1 and CERT to acquire host sphingomyelin for distinct roles during intracellular development. PLoS Pathog 7:e1002198.

Follit JA, Tuft RA, Fogarty KE, Pazour GJ. 2006. The intraflagellar transport protein IFT20 is associated with the Golgi complex and is required for cilia assembly. Mol Biol Cell 17:3781–3792.

Follit JA, San Agustin JT, Xu F, Jonassen JA, Samtani R, Lo CW, Pazour GJ. 2008. The Golgin GMAP210/TRIP11 anchors IFT20 to the Golgi complex. PLoS Genet 4:e1000315.

Gabel BR, Elwell C, van Ijzendoorn SC, Engel JN. 2004. Lipid raft-mediated entry is not required for *Chlamydia trachomatis* infection of cultured epithelial cells. Infect Immun 72:7367–7373.

Gaietta GM, Giepmans BN, Deerinck TJ, Smith WB, Ngan L, Llopis J, Adams SR, Tsien RY, Ellisman MH. 2006. Golgi twins in late mitosis revealed by genetically encoded tags for live cell imaging and correlated electron microscopy. Proc Natl Acad Sci USA 103:17777–17782.

Greene W, Zhong G. 2003. Inhibition of host cell cytokinesis by *Chlamydia trachomatis* infection. J Infect 47:45–51.

Hackstadt T, Scidmore MA, Rockey DD. 1995. Lipid metabolism in *Chlamydia trachomatis*-infected cells: Directed trafficking of Golgi-derived sphingolipids to the chlamydial inclusion. Proc Natl Acad Sci USA 92:4877–4881.

Hackstadt T, Rockey DD, Heinzen RA, Scidmore MA. 1996. *Chlamydia trachomatis* interrupts an exocytic pathway to acquire endogenously synthesized sphingomyelin in transit from the Golgi apparatus to the plasma membrane. Embo J 15:964–977.

Hackstadt T, Fischer ER, Scidmore MA, Rockey DD, Heinzen RA. 1997. Origins and functions of the chlamydial inclusion. Trends Microbiol 5:288–293.

Hatch TP, Allan I, Pearce JH. 1984. Structural and polypeptide differences between envelopes of infective and reproductive life cycle forms of Chlamydia spp. J Bacteriol 157:13–20.

Hatch TP. 1975. Utilization of L-cell nucleoside triphosphates by Chlamydia psittaci for ribonucleic acid synthesis. J Bacteriol 122:393–400.

Heuer D, Lipinski AR, Machuy N, Karlas A, Wehrens A, Siedler F, Brinkmann V, Meyer TF. 2009. Chlamydia causes fragmentation of the Golgi compartment to ensure reproduction. Nature 457:731–735.

Hybiske K, Stephens RS. 2007. Mechanisms of host cell exit by the intracellular bacterium Chlamydia. Proc Natl Acad Sci USA 104:11430–11435.

Jiang S, Rhee SW, Gleeson PA, Storrie B. 2006. Capacity of the Golgi apparatus for cargo transport prior to complete assembly. Mol Biol Cell 17:4105–4117.

Jutras I, Abrami L, Dautry-Varsat A. 2003. Entry of the lymphogranuloma venereum strain of *Chlamydia trachomatis* into host cells involves cholesterol-rich membrane domains. Infect Immun 71:260–266.

Kari L, Goheen MM, Randall LB, Taylor LD, Carlson JH, Whitmire WM, Virok D, Rajaram K, Endresz V, McClarty G, Nelson DE, Caldwell HD. 2011. Generation of targeted *Chlamydia trachomatis* null mutants. Proc Natl Acad Sci USA 108:7189–7193.

Knowlton AE, Brown HM, Richards TS, Andreolas LA, Patel RK, Grieshaber SS. 2011. *Chlamydia trachomatis* infection causes mitotic spindle pole defects independently from its effects on centrosome amplification. Traffic 12:854–866.

Knowlton AE, Fowler LJ, Patel RK, Wallet SM, Grieshaber SS. 2013. Chlamydia induces anchorage independence in 3T3 cells and detrimental cytological defects in an infection model. PLoS ONE 8:e54022.

Liu J, Fairn GD, Ceccarelli DF, Sicheri F, Wilde A. 2012. Cleavage furrow organization requires PIP(2)-mediated recruitment of anillin. Curr Biol 22:64–69.

Madeleine MM, Anttila T, Schwartz SM, Saikku P, Leinonen M, Carter JJ, Wurscher M, Johnson LG, Galloway DA, Daling JR. 2007. Risk of cervical cancer associated with *Chlamydia trachomatis* antibodies by histology, HPV type and HPV cofactors. Int J Cancer 120:650–655.

Mital J, Miller NJ, Fischer ER, Hackstadt T. 2010. Specific chlamydial inclusion membrane proteins associate with active Src family kinases in microdomains that interact with the host microtubule network. Cell Microbiol 12:1235–1249.

Neeper ID, Patton DL, Kuo CC. 1990. Cinematographic observations of growth cycles of *Chlamydia trachomatis* in primary cultures of human amniotic cells. Infect Immun 58:2042–2047.

Pagano RE, Martin OC, Kang HC, Haugland RP. 1991. A novel fluorescent ceramide analogue for studying membrane traffic in animal cells: Accumulation at the Golgi apparatus results in altered spectral properties of the sphingolipid precursor. J Cell Biol 113:1267–1279.

Piekny AJ, Glotzer M. 2008. Anillin is a scaffold protein that links RhoA, actin, and myosin during cytokinesis. Curr Biol 18:30–36.

Rejman Lipinski A, Heymann J, Meissner C, Karlas A, Brinkmann V, Meyer TF, Heuer D. 2009. Rab6 and Rab11 regulate *Chlamydia trachomatis* development and golgin-84-dependent Golgi fragmentation. PLoS Pathog 5:e1000615.

Shima DT, Cabrera-Poch N, Pepperkok R, Warren G. 1998. An ordered inheritance strategy for the Golgi apparatus: Visualization of mitotic disassembly reveals a role for the mitotic spindle. J Cell Biol 141:955–966.

Su KC, Takaki T, Petronczki M. 2011. Targeting of the RhoGEF Ect2 to the equatorial membrane controls cleavage furrow formation during cytokinesis. Dev Cell 21:1104–1115.

Sun HS, Wilde A, Harrison RE. 2011. *Chlamydia trachomatis* inclusions induce asymmetric cleavage furrow formation and ingression failure in host cells. Mol Cell Biol 31:5011–5022.

Sun HS, Eng EW, Jeganathan S, Sin AT, Patel PC, Gracey E, Inman RD, Terebiznik MR, Harrison RE. 2012. *Chlamydia trachomatis* vacuole maturation in infected macrophages. J Leukoc Biol 92:815–827.

Suzaki E, Kataoka K. 1992. Lectin cytochemistry in the gastrointestinal tract with special reference to glycosylation in the Golgi apparatus of Brunner's gland cells. J Histochem Cytochem 40:379–385.

Tipples G, McClarty G. 1993. The obligate intracellular bacterium *Chlamydia trachomatis* is auxotrophic for three of the four ribonucleoside triphosphates. Mol Microbiol 8:1105–1114.

Velasco A, Hendricks L, Moremen KW, Tulsiani DR, Touster O, Farquhar MG. 1993. Cell type-dependent variations in the subcellular distribution of alpha-mannosidase I and II. J Cell Biol 122:39–51.

Wang Y, Kahane S, Cutcliffe LT, Skilton RJ, Lambden PR, Clarke IN. 2011. Development of a transformation system for *Chlamydia trachomatis*: Restoration of glycogen biosynthesis by acquisition of a plasmid shuttle vector. PLoS Pathog 7:e1002258.

Wasano K, Nakamura K, Yamamoto T. 1988. Lectin-gold cytochemistry of mucin oligosaccharide biosynthesis in Golgi apparatus of airway secretory cells of the hamster. Anat Rec 221:635–644.

Wei JH, Seemann J. 2009. The mitotic spindle mediates inheritance of the Golgi ribbon structure. J Cell Biol 184:391–397.

Whitfield ML, Sherlock G, Saldanha AJ, Murray JI, Ball CA, Alexander KE, Matese JC, Perou CM, Hurt MM, Brown PO, Botstein D. 2002. Identification of genes periodically expressed in the human cell cycle and their expression in tumors. Mol Biol Cell 13:1977–2000.

WHO. 2001. Global prevalence and incidence of selected curable sexually transmitted infections: Overview and estimates. Geneva: World Health Organization.

SUPPORTING INFORMATION

Additional supporting information may be found in the online version of this article at the publisher's web-site.